Flipped Out: Structure-Guided Design of Selective Pyrazolylpyrrole ERK Inhibitors[‡]

Alex M. Aronov,* Christopher Baker, Guy W. Bemis, Jingrong Cao, Guanjing Chen, Pamella J. Ford, Ursula A. Germann, Jeremy Green, Michael R. Hale, Marc Jacobs, James W. Janetka, Francois Maltais, Gabriel Martinez-Botella, Mark N. Namchuk, Judy Straub, Qing Tang, and Xiaoling Xie

Vertex Pharmaceuticals Inc., 130 Waverly Street, Cambridge, Massachusetts 02139-4242

The Ras/Raf/MEK/ERK signal transduction is a key oncogenic pathway implicated in a variety of human cancers. We have identified a novel series of pyrazolylpyrroles as inhibitors of ERK. Aided by the discovery of two distinct binding modes for the pyrazolylpyrrole scaffold, structure-guided optimization culminated in the discovery of **6p**, a potent and selective inhibitor of ERK.

Introduction

Cancer has surpassed heart disease as the leading cause of death in the U.S. for persons younger than 85.[1] For most types of cancer, chemotherapeutic treatments have achieved limited success to date and highlight the need for more efficacious, better-tolerated therapy. Improved understanding of cancer biology at the molecular level has led to a shift in treatment paradigm from the traditional cytotoxics toward more rationally designed targeted therapies. These target molecular lesions that are deregulated in cancer, primarily oncoproteins and oncogenic pathways. Examples of molecular targets in cancer include overexpression of receptor tyrosine kinases (RTKs[a]) or mutants thereof (such as BCR-ABL,[2] EGFR,[3] ErbB2,[4] and FLT3[5]), as well as activating mutations in the Ras GTPase proteins[6] or B-Raf.[7]

A common feature of many deregulated molecular lesions in cancer is the activation of the Ras/Raf/MEK/ERK signal transduction pathway (hereafter referred to as the ERK pathway). This pathway controls a number of fundamental cellular processes including cell survival, proliferation, motility, and differentiation.[8−12] It is constitutively activated in cancers of the lung, colon, pancreas, kidney, and ovary. Furthermore, some of the best characterized oncogenic mutations (e.g., Ras, B-Raf) reside in the ERK pathway. A number of companies have targeted ERK pathway blockers. Sorafenib (Nexavar),[13] an inhibitor of Raf kinase along with a number of RTKs, was approved in late 2005 for the treatment of renal cell carcinoma. Two highly selective ATP-noncompetitive inhibitors of ERK-activating kinase MEK, PD-0325901 (Pfizer),[14] and ARRY-142886/AZD6244 (Array/AstraZeneca)[15] are currently undergoing clinical development.[13]

ERK is pivotal in the pathway downstream of Ras, Raf, and MEK, acting as a central point where multiple signaling pathways coalesce to drive transcription. ERK1 and ERK2 share 88% sequence identity, and the residues in the ATP site are conserved. Our goal was to design novel and selective ATP competitive inhibitors of ERK that would enable control over the penultimate step in this key signal transduction pathway.
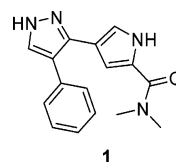
Figure 1. Structure of ERK2 screening hit **1**.
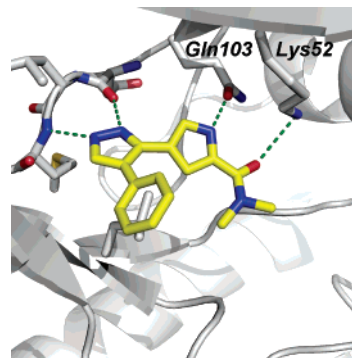

Figure 2. Crystal structure of ERK2 bound to screening hit **1**.

This report describes our efforts in combining X-ray crystallography, molecular modeling, and medicinal chemistry toward the discovery and optimization of pyrazolylpyrroles as a novel selective series of ERK1,2 inhibitors.

In the course of an initial high throughput screen pyrazolylpyrrole **1** (Figure 1) was discovered as a micromolar inhibitor of ERK (K_I = 2.3 μM). Kinase activity of pyrazolylpyrroles has been reported previously.[16−18] We initiated crystallographic studies of **1** complexed to ERK to further our structural understanding of the key binding elements responsible for its ERK inhibition. The resulting X-ray structure (Figure 2) revealed that the pyrazole ring of **1** was critical to its activity, making two hydrogen bonds to the hinge region of ERK. The amide carbonyl of **1** formed a hydrogen bond with the catalytic Lys52, and the pyrazole-linked phenyl made a hydrophobic interaction with Val37 of the glycine-rich loop. Finally, the pyrrole NH was involved in a hydrogen bond with the side-chain carbonyl of the gatekeeper residue Gln103. The gatekeeper residue has a well-established role in determining the selectivity of kinase inhibitors.[19] Based on this structural information, we chose to vary substituents on the phenyl and the amide, where additional space was available, while keeping the pyrazolylpyrrole amide core of **1** intact.

Scheme 1[a]
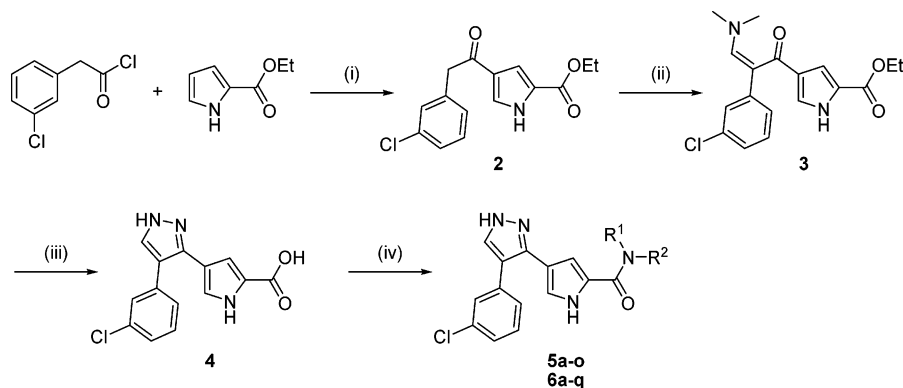
[a] Reagents: (i) AlCl$_3$, CH$_2$Cl$_2$; (ii) *t*-BuOCH(NMe$_2$)$_2$, DMF; (iii) (a) N$_2$H$_4$, DMF; (b) 50% NaOH in EtOH; (iv) EDCI, HOBT, DIEA, DMF, R^{1}R^{2}NH.

Chemistry. Pyrazolylpyrrole carboxamides were prepared in a four step procedure (Scheme 1). A Friedel–Crafts acylation of commercially available ethyl pyrrole-2-carboxylate produced ketone **2**. Treatment of **2** with Bredereck's reagent followed by cyclization with hydrazine afforded carboxylic acid **4** after hydrolysis of the ethyl ester. A standard coupling procedure with EDCI furnished the desired analogs **5** and **6**.

Results and Discussion

We first proceeded to introduce small, mostly lipophilic substituents into the phenyl ring of **1** to optimize the interaction with the glycine-rich loop (data not shown). 3-Chlorophenyl afforded a 3-fold improvement in activity over **1**, and the subsequent work described in the present communication includes this substituent throughout.

The pyrrole carboxamide portion of the scaffold provided a straightforward entry for diversity generation from a list of available amines. The amide projects into the salt bridge area of the ATP site between Lys52 and Asp165, making ample space available to accommodate the amide substituents. Cyclization of the amide fragment in **5b** and **5c** did not provide any advantage over uncyclized tertiary amides, such as **5a**. Surprisingly, introduction of a basic *N*-ethylpyrrolidine moiety (**5e**) resulted in a complete loss of ERK activity, despite its special proximity to carboxylate of Asp165. Aliphatic amides were preferred over aromatics, with anilide **5f** losing 10-fold relative to pyrrolidine amide **5b**, likely due to the steric clash with Asp165 incurred by the planar amide extension. The biggest ERK K_I improvement was observed in the case of benzylamide **5g** (K_I = 86 nM). A number of modifications to the benzyl fragment were detrimental to ERK activity to varying degrees. The *m/p*-picolyl amides **5h** and **5i** were 3- and 2-fold less active than **5g**, respectively, likely due to unfavorable interactions with the hydrophobic pocket bounded by the glycine-rich loop. Amide methylation of **5g** resulted in a 5-fold drop in potency (**5j**). Both rigidification of benzylamide to tetrahydroisoquinoline **5m** and elongation of the linker to hydroxamate ester **5o** led to a loss in activity. However, hydrophobic substitution of the benzyl moiety (2,3-difluoro-, **5k**) led to a further 2-fold potency improvement.

The activity of the pyrazolylpyrroles against JNK3 was established early as the main selectivity concern for the series. As seen in Table 1, most pyrazolylpyrrole carboxamides afforded a selectivity window of less than 10-fold between ERK2 and JNK3. The selectivity increased to approximately 20-fold in the case of **5k**, and we chose to collect structural information that would allow to better differentiate between ERK and JNK.

Table 1. Activity of Pyrrole Carboxamide Analogs of **1**

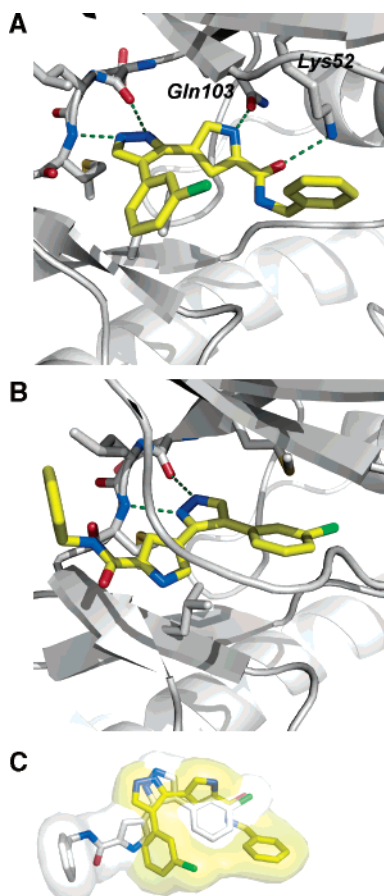| Compound	R$_1$	R$_2$	ERK2 K_I, μM	JNK3 K_I, μM
1	H	NMe2	2.3	> 4
5a	Cl	N(Me)Et	0.58	> 4
5b	Cl	—N(pyrrolidine)	0.20	1.8
5c	Cl	—N(morpholine)	0.87	> 4
5d	Cl	—NH-CH$_2$-(tetrahydrofuran)	0.43	2.7
5e	Cl	—NH-(N-ethylpyrrolidine)	> 10	> 4
5f	Cl	—NH-phenyl	2.0	ND[a]
5g	Cl	—NH-CH$_2$-phenyl	0.086	0.55
5h	Cl	—NH-CH$_2$-(3-pyridyl)	0.23	ND
5i	Cl	—NH-CH$_2$-(4-pyridyl)	0.16	ND
5j	Cl	—N(Me)-CH$_2$-phenyl	0.44	> 4
5k	Cl	—NH-CH$_2$-(2,3-difluorophenyl)	0.040	0.79
5l	Cl	—NH-CH$_2$-(4-methoxyphenyl)	0.49	0.84
5m	Cl	—N(tetrahydroisoquinoline)	0.51	> 4
5n	Cl	—NH-CH$_2$-(3-pyridyl)	0.33	> 4
5o	Cl	—O-NH-CH$_2$-phenyl	0.17	2.9

[a] ND = not determined.

Figure 3. Structural characterization of the binding of **5g** to kinases. (A) Crystal structure of **5g** bound to ERK2. (B) Crystal structure of **5g** bound to JNK3. (C) Overlay of the binding modes of **5g** in ERK2 (yellow) and JNK3 (white).

Figure 4. Crystal structure of selective ERK2 inhibitor **6p** bound to ERK2. (A) Hydrogen-bonding pattern in the structure of **6p** bound to ERK2. (B) Steric fit of **6p** within the ERK2 active site.

The crystal structure of **5g** bound to ERK2 (Figure 3A) was largely consistent with the previously obtained structure of **1**. The four hydrogen bonds observed for **1** were all present. As expected, the 3-chloro substituent was in contact with Val37. Finally, the benzyl moiety of **5g** pointed toward the glycine-rich loop, while making favorable hydrophobic contacts with the Cδ of Lys52 side chain, which likely explains its higher ERK activity. Open space near the *m/p*-positions of the benzyl explained the activity of **5k**, pointing toward a potential for more favorable interactions in that region of the active site.

The crystal structure of **5g** bound to JNK3 was sought to explain the rather consistent inhibition of JNK by the pyrazolylpyrroles and to provide guidance for eliminating this undesirable activity. To our surprise, the binding mode of **5g** in the active site of JNK3 (Figure 3B) was dramatically different from the previously observed ERK binding mode (Figures 2 and 3A). Indeed, the conformation and orientation of **5g** bound to JNK was almost exactly opposite of the ERK-bound conformation (Figure 3B,C). Two hydrogens bonds were observed between the pyrazole core of **5g** and the hinge region of JNK, however, both were made by the alternate tautomer of the pyrazole ring. Correspondingly, the pyrrole and the chlorophenyl substituents effectively swapped places within the ATP site. The chlorophenyl was observed in proximity to Lys52, while the pyrrole carboxamide straddled the hinge of JNK3 out toward solvent.

Based on the difference between the two binding modes, we hypothesized that the addition of a polar group containing a hydrogen bond donor to the benzylic methylene of **5g** should
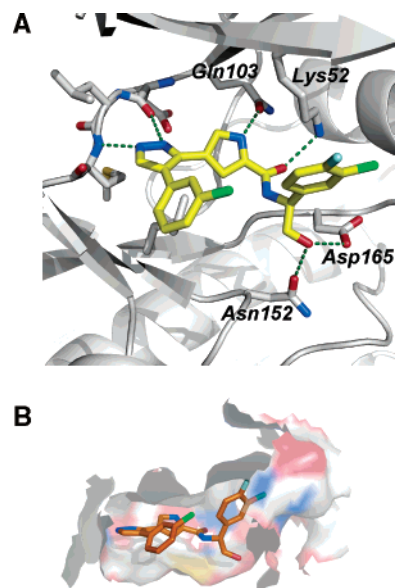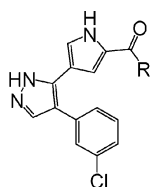
be particularly beneficial for the ERK-bound conformation of **5g**. The side chain carboxylate of Asp165 and the amide carbonyl of Asn152 both place their sp2 oxygens in the vicinity of the benzylic position and would be expected to form a favorable interaction with a donor moiety. In contrast, the benzylic carbon of **5g** is in Van der Waals contact with main chain atoms of Asp150 in the JNK3-bound structure, with branching predicted to be detrimental for JNK activity. We expected (*R*)-stereochemistry to be preferred for the benzylic carbon—it is positioned within 3.7 Å of the Asp165 side chain on the pro-(*S*) side. To confirm the desired stereochemistry at the benzylic position, chiral methyl benzamides **6a** and **6b** were prepared (Table 2). Indeed, the (*R*)-enantiomer **6a** was equipotent with **5g**, while (*S*)-methyl led to a 7-fold drop in activity. Importantly, selectivity of **6a** against JNK3 improved to 30-fold, compared to only 6-fold for **5g**. Validating our structural observations, the hydroxyl donor-containing (*S*)-phenylglycinol **6c** led to a further 3-fold improvement in ERK K_I relative to **6a**, from 100 nM to 35 nM. As expected, placement of a carboxylate in proximity to Asp165 resulted in a loss of ERK activity for **6d**. Reintroduction of hydrogen bond donors as the primary amide (**6e**) regained some of the activity lost by **6d**, but additional steric bulk (**6f**) predictably interfered with hydrogen bond formation. Rigidification of the glycinol moiety into indane **6g** led to 100-fold loss in ERK activity.

The final optimization step involved exploration of substituent effects on the phenyl moiety of phenylglycinol, using (*S*)-phenylglycinol **6c** (K_I = 35 nM) as a benchmark. As seen from our previous efforts around **5g** (Table 1), hydrophobic substitutions such as 3,4-difluoro (**5k**) were expected to be preferred for phenylglycinols as well. At the *para*-position of phenyl, the 4-chloro substituent in **6i** was optimal (K_I = 14 nM), with both a smaller 4-fluoro and a larger 4-CF$_3$ dropping off by 3- to 4-fold in potency. The *ortho*-substituent was not well tolerated in **6k**, while introduction of 3-fluoro afforded **6l** (K_I = 24 nM). Dihalogenated phenylglycinols **6m−o** provided the most active compounds in the series. Finally, the (*S*)-enantiomer **6p** was the most potent compound synthesized, with ERK K_I = 2 nM, 43-fold more potent that **5g**. Remarkably, it maintained its selectivity over JNK3 (K_I > 4 μM). The

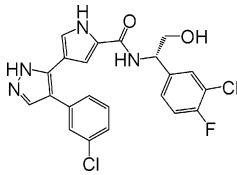**Table 2.** Activity of Pyrrole Carboxamide Analogs of **5g**

Cmpd	R	ERK2 K_i, µM	JNK3 K_i, µM	Cmpd	R	ERK2 K_i, µM	JNK3 K_i, µM
5g	—NH–benzyl	0.086	0.55	**6i**	—NH–CH(CH₂OH)–C₆H₄–Cl	0.014	2.5
6a	—NH–CH(CH₃)–phenyl	0.10	3.1	**6j**	—NH–CH(CH₂OH)–C₆H₄–CF₃	0.044	2.7
6b	—NH–CH(CH₃)–phenyl	0.66	> 4	**6k**	—NH–CH(CH₂OH)–(2-F)phenyl	0.24	3.1
6c	—NH–CH(CH₂OH)–phenyl	0.035	2.8	**6l**	—NH–CH(CH₂OH)–(3-F)phenyl	0.024	3.0
6d	—NH–CH(CO₂H)–phenyl	> 5	> 4	**6m**	—NH–CH(CH₂OH)–(3,4-diF)phenyl	0.022	2.8
6e	—NH–CH(C(=O)NH₂)–phenyl	0.51	3.3	**6n**	—NH–CH(CH₂OH)–(3,5-diCl)phenyl	0.007	3.4
6f	—NH–CH(C(=O)NHCH₃)–phenyl	2.3	3.9	**6o**	—NH–CH(CH₂OH)–(3-Cl,4-F)phenyl	0.006	ND[a]
6g	—NH–(2-hydroxyindanyl)	4.0	3.2	**6p**	—NH–CH(CH₂OH)–(3-Cl,4-F)phenyl	0.002	> 4
6h	—NH–CH(CH₂OH)–(4-F)phenyl	0.063	> 4	**6q**	—NH–CH(CH₂OH)–(3-Cl,4-F)phenyl	0.15	> 4

[a] ND = not determined.

corresponding (*R*)-enantiomer **6q** was approximately 70-fold less active than **6p**.

The kinase counterscreening profile of **6p** is shown in Table 3. The compound is about 200-fold selective against PKA, the smallest selectivity window of all kinases tested, and is active in the Colo205 cell proliferation assay (IC₅₀ = 0.54 µM). Encouraged by the ERK-selective kinase activity profile of **6p**, we pursued the crystal structure of the **6p**−ERK2 complex as further validation of our structure-guided optimization strategy. The structure shown in Figure 4A confirmed the presence of two additional hydrogen bonds made by the hydroxyl of (*S*)-phenylglycinol in the salt bridge area of the ATP site to the carboxylate oxygen of the Asp165 as well as the carboxamide oxygen of the Asn152 side chain. In addition, four hydrogen bonds observed previously for **1** and **5g** were also present, such that six hydrogen bonds now anchor **6p** within the ERK2 active site. The halogen substituents on the phenylglycinol fill the hydrophobic cavity (Figure 4B) and provide favorable interactions with the glycine-rich loop of ERK. The favorable stereochemistry of (*S*)-phenylglycinol is determined by the geometry of the site—(*R*)-stereochemistry at this position would interfere with the side chain of Asp165, which lies within 4 Å of the benzylic carbon of **6p**. It appears that the combination of hydrogen bonds to the hinge and the salt bridge portion of the ERK2 active site, coupled to the interactions with the glycine-rich loop provided by the three halogens in **6p**, and the additional hydrogen bond to the gatekeeper Gln103 are responsible for the potency and ERK selectivity displayed by **6p**.

Table 3. Kinase Counterscreening Data and Cellular Activity for **6p**

assay	$K_I, \mu M$
ERK2	0.002
PKA	0.39
FLT3	0.75
SRC	1.1
LCK	1.2
AKT3	1.8
GSK3	3.3
KDR	3.9
JNK3	4
AURA	>4
CDK2	>4
MEK1	>4
P38α	>4
Colo205	0.54[a]

[a] IC_{50} in the Colo205 proliferation assay (see Supporting Information for details).

Conclusion

We have designed a series of selective and potent inhibitors of ERK kinase by starting with a micromolar lead compound **1**, followed by several rounds of structure-guided optimization. In particular, selectivity against JNK3 was optimized following the discovery of two alternative binding modes assumed by the pyrazolylpyrrole inhibitors. Stabilizing the ERK-bound orientation of **5g** by introducing additional functionality, we were able to ultimately design **6p**, a selective nanomolar ERK2 inhibitor.

This study is one of only a few examples in the literature of compounds assuming different binding modes when bound to two distinct kinases. The best known case to date is the ability of imatinib to inhibit ABL[20] and SYK[21] by binding to these kinases in two drastically different conformations/orientations. Both imatinib binding conformations have been shown to be important in the recognition of other protein kinases—imatinib binds to KIT in the ABL-like mode,[22] while its des-methyl analog assumes the SYK-like conformation for binding to Src.[23] In our experience, this observation is not uncommon, and we expect future crystallographic studies with known inhibitors to produce more examples of the "multiple binding modes" phenomenon.

Experimental Section

General Experimental Details. All commercial reagents and anhydrous solvents were obtained from commercial sources and were used without further purification, unless otherwise specified. Mass samples were analyzed on a Micro Mass ZQ, ZMD, Quattro LC, or Quatro II mass spectrometer operated in a single MS mode with electrospray ionization. Samples were introduced into the mass spectrometer using flow injection (FIA) or chromatography. The mobile phase for all mass analysis consisted of acetonitrile—water mixtures with either 0.2% formic acid or ammonium formate. The high-resolution mass spectrum was measured using a 9.4T APEX III FTMS Bruker Daltonics instrument. The following HPLC methods were used to obtain the reported retention times. (i) **Method A:** YMC ProC18 column, 2.0 × 50 mm; linear gradient from 0% to 90% CH₃CN in H₂O over 4 min (0.1% trifluoroacetic acid); flow rate 0.8 mL/min; 214 nM/254 nM. (ii) **Method B:** Water Symmetry C18 column, 4.6 50 mm; linear gradient from 10% to 90% CH₃CN in H₂O over 3 min (0.2% formic acid); flow rate 1.5

mL/min; detection diode array. (iii) **Method C:** Water Symmetry C18 column, 4.6 × 50 mm; linear gradient from 2% to 90% CH₃-CN in H₂O over 3 min (2% ammonium formate); flow rate 1.5 mL/min; detection diode array. (iv) **Method D:** YMC ODS-AQ 5 μm 120A column, 3.0 × 150 mm; linear gradient 10% to 90% CH₃CN in H₂O over 8 min (0.1% trifluoroacetic acid); flow rate 1.0 mL/min; 214 nM. (vi) **Method E:** YMC ProC18 column, 2.0 × 50 mm; linear gradient from 10% to 90% CH₃CN in H₂O over 5 min (0.2% formic acid); flow rate 1.5 mL/min; detection diode array. (v) **Method F:** YMC ODS-AQ 5 μm 120A column, 3.0 × 150 mm; linear gradient from 10% to 90% CH₃CN in H₂O over 22 min (0.1% trifluoroacetic acid); flow rate 1.0 mL/min; 214 nM. (vi) **Method G:** YMC ODS-AQ 5 μm 120A column, 3.0 × 150 mm; linear gradient from 15% to 90% CH₃CN in H₂O over 10 min (0.2% trifluoroacetic acid); flow rate 1.5 mL/min; detection diode array. ¹H NMR spectra (δ, ppm) was recorded either using a Bruker DRX-500 (500 MHz) or a Bruker Avance II-300 (300 MHz) instrument. Elemental analyses were performed by Quantitative Technologies, Inc. Column chromatography was performed using Merck silica gel 60 (0.040−0.063 mm). Preparative reversed-phase chromatography was carried out using a Gilson 215 liquid handler coupled to a UV−vis 156 Gilson detector, an Agilent Zorbax SB-C18 column, 21.2 × 100 mm, a linear gradient from 10% to 90% CH₃CN in H₂O over 10 min (0.1% trifluoroacetic acid); flow rate 20 mL/min. 2-(3-Chlorophenyl)acetyl chloride was synthesized following literature procedures.[24] Most amines are commercially available, except for the following: (i) the amine in **6f**, which was obtained following literature procedures[25] and (ii) the amines in **6j**, **6o**, **6p**, **6q** were obtained from the corresponding substituted phenylalanines after reduction with borane[26] (data not shown).

Ethyl 4-(2-(3-Chlorophenyl)acetyl)-1*H*-pyrrole-2-carboxylate (2). To a solution of 2-(3-chlorophenyl)acetyl chloride (19.9 g, 105 mmol) and ethyl 1*H*-pyrrole-2-carboxylate (11.3 g, 81 mmol) in dichloromethane (100 mL) at 0 °C, AlCl₃ (32 g, 243 mmol) was added in small batches. The reaction mixture was allowed to warmed up to room temperature overnight. The crude was poured onto ice and extracted with dichloromethane. After drying over anhydrous sodium sulfate and removing the solvent under reduced pressure, the crude product was purified by flash chromatography on silica gel, eluting with dichloromethane and methanol (3%). The title compound **2** was isolated as a solid (23 g, 99%). HPLC (Method F) t_R = 10.07 min; ¹H NMR (500 MHz, CDCl₃) δ 10.15 (br s, 1H), 7.5 (d, 1H), 7.35 (s, 1H), 7.30−7.15 (m, 3H), 7.1 (d, 1H), 4.35 (q, 2H), 4.1 (s, 2H), 1.4 (t, 3H).

Ethyl 4-(2-(3-Chlorophenyl)-3-(dimethylamino)acryloyl)-1*H*-pyrrole-2-carboxylate (3). To a solution of **2** (23 g, 79 mmol) in DMF (40 mL), *tert*-butoxy-*N,N,N′,N′*-tetramethanediamine (29.6 g, 170 mmol) was added, and the resulting mixture was stirred overnight at room temperature. The crude product was dissolved in ethyl acetate and washed with water. After drying over anhydrous sodium sulfate, the solvent was removed under reduced pressure, and the resulting oil **3** was dried under vacuum overnight and used in the next step without further purification. HPLC (Method F) t_R = 13.77 min.

Ethyl 4-(4-(3-Chlorophenyl)-1*H*-pyrazol-3-yl)-1*H*-pyrrole-2-carboxylate (7). To a solution of **3** (79 mmol) in DMF (40 mL), hydrazine hydrate (4.05 g, 81 mmol) was added, and the resulting mixture was warmed at 60 °C overnight. The mixture was diluted in ethyl acetate and washed with water. After removing the solvent under reduced pressure, the crude was purified by flash chromatography on silica gel, eluting with dichloromethane and methanol (3%), yielding the title compound **7** (20 g, 78%). HPLC (Method F) t_R = 10.25 min; LC-MS (Method G) t_R = 7.4 min, 316.2 (M + 1), 314.2 (M − 1); ¹H NMR (500 MHz, CDCl₃) δ 10.3 (br s, 1H), 7.75 (s, 1H), 7.45 (s, 1H), 7.30−7.20 (m, 3H), 7.1 (d, 1H), 7.05 (d, 1H), 4.35 (q, 2H), 4.1 (s, 2H), 1.3 (t, 3H).

4-(4-(3-Chlorophenyl)-1*H*-pyrazol-3-yl)-1*H*-pyrrole-2-carboxylic Acid (4). To a solution of **7** (2.3 g, 7.2 mmol) in ethanol (50 mL), aqueous NaOH (50%; 1 mL) was added, and the resulting mixture was warmed at 60 °C overnight. The solvent was removed

under reduced pressure, and the crude was dissolved in ethyl acetate and water. The water layer was washed with ethyl acetate (3 × 50 mL). The aqueous layer was then acidified to pH = 3 and then extracted with ethyl acetate. The organic fraction was dried over magnesium sulfate, and the solvent was removed under reduced pressure. The desired acid **4** was isolated and used without further purification (1.72 g, 83%). HPLC (Method F) t_R = 8.59 min; LC-MS (Method B) t_R = 2.79 min, 288.4 (M + 1), 286.3 (M − 1); ^{1}H NMR (300 MHz, DMSO-d_6) δ 12.9 (br s, 2H), 11.9 (br s, 1H), 7.88 (s, 1H), 7.40−7.27 (m, 4H), 7.0 (s, 1H), 6.78 (s, 1H); HRMS calcd for $C_{14}H_{10}ClN_3O_2$+H, 288.0534; found, 288.0534.

General Method for the Synthesis of Amides 5a−5o and 6a− 6q. The acid **4** (30 mg, 0.10 mmol), EDCI (24 mg, 0.12 mmol), HOBt (17 mg, 0.12 mmol), DIEA (73 μL, 0.4 mmol), and the desired amine (1.2 equiv) were combined in dichloromethane (2 mL) and stirred at room temperature for 2−16 h. The solvent was then removed under reduced pressure, and the resulting crude was dissolved in ethyl acetate, washed with 0.5 N aqueous HCl, saturated aqueous sodium bicarbonate, and brine, and then dried over anhydrous magnesium sulfate. After removing the solvent under reduced pressure, the crude product was purified by reversed-phase chromatography. Samples were isolated as TFA salts after lyophilizing.

4-(4-(3-Chlorophenyl)-1*H*-pyrazol-3-yl)-*N*-ethyl-*N*-methyl-1*H*-pyrrole-2-carboxamide (5a). HPLC (Method A) t_R = 3.23 min; LC-MS (Method B) t_R = 3.0 min, 329.4 (M + 1), 327.4 (M − 1); LC-MS (Method C) t_R = 2.7 min, 329.1 (M + 1), 327.2 (M − 1); HRMS calcd for $C_{17}H_{17}ClN_4O$+H, 329.1164; found, 329.1166.

4-(4-(3-Chlorophenyl)-1*H*-pyrazol-3-yl)-1*H*-pyrrol-2-yl)(pyr-rolidin-1-yl)methanone (5b). HPLC (Method A) t_R = 3.27 min; LC-MS (Method B) t_R = 3.0 min, 341.5 (M + 1), 339.4 (M − 1); LC-MS (Method C) t_R = 2.7 min, 341.1 (M + 1), 339.2 (M − 1); ^{1}H NMR (300 MHz, DMSO-d_6) δ 11.65 (s, 1H), 7.75 (s, 1H), 7.47 (br t, 1H), 7.39−7.37 (m, 2H), 7.32−7.28 (m, 1H), 6.99 (m, 1H), 6.70 (br t, 1H), 3.58 (br t, 2H), 3.47 (br t, 2H), 1.92−1.81 (m, 4H); HRMS calcd for $C_{18}H_{17}ClN_4O$+H, 341.1164; found, 341.1165. Anal. Calcd for $C_{20}H_{18}ClF_3N_4O_3$·0.5H_2O: C, 51.79; H, 4.13; N, 12.08. Found: C, 51.56; H, 4.03; N, 11.91.

4-(4-(3-Chlorophenyl)-1*H*-pyrazol-3-yl)-1*H*-pyrrol-2-yl)(mor-pholino)methanone (5c). HPLC (Method A) t_R = 3.07 min; LC-MS (Method B) t_R = 2.7 min, 357.5 (M + 1), 355.5 (M − 1); LC-MS (Method C) t_R = 2.5 min, 357.2 (M + 1), 355.3 (M − 1); ^{1}H NMR (500 MHz, CDCl$_3$) δ 10.3 (br s, 1H), 7.7 (s, 1H), 7.4 (s, 1H), 7.3 (m, 4H), 7.1 (s, 1H), 6.5 (s, 1H), 3.8 (m, 4H), 3.65 (m, 4H); HRMS calcd for $C_{18}H_{17}ClN_4O_2$+H, 357.1113; found, 357.1112. Anal. Calcd for $C_{18}H_{17}ClN_4O_2$·0.5CF_3CO_2H·H_2O: C, 52.85; H, 4.55; N, 12.97. Found: C, 52.92; H, 4.40; N, 12.70.

4-(4-(3-Chlorophenyl)-1*H*-pyrazol-3-yl)-*N*-((tetrahydrofuran-2-yl)methyl)-1*H*-pyrrole-2-carboxamide (5d). HPLC (Method A) t_R = 3.14 min; LC-MS (Method B) t_R = 2.8 min, 371.5 (M + 1), 369.5 (M − 1); LC-MS (Method C) t_R = 2.6 min, 371.2 (M + 1), 369.3 (M − 1); ^{1}H NMR (300 MHz, DMSO-d_6) δ 11.65 (s, 1H), 8.12 (t, J = 5.1 Hz 1H), 7.78 (s, 1H), 7.43 (br s, 1H), 7.34 (br d, 2H), 7.32−7.25 (m, 1H), 6.94 (br m, 1H), 6.90 (br t, 1H), 3.92 (m, 1H), 3.8 (m, obscured by H$_2$O), 3.22 (q, 2H), 1.93−1.86 (m, 3H), 1.61−1.51 (m, 1H); HRMS calcd for $C_{19}H_{19}ClN_4O_2$+H, 371.1269; found, 371.1271.

4-(4-(3-Chlorophenyl)-1*H*-pyrazol-3-yl)-*N*-((1-ethylpyrrolidin-2-yl)methyl)-1*H*-pyrrole-2-carboxamide (5e). HPLC (Method A) t_R = 2.78 min; LC-MS (Method B) t_R = 2.3 min, 398.6 (M + 1); LC-MS (Method C) t_R = 2.6 min, 398.2 (M + 1), 396.3 (M − 1); ^{1}H NMR (300 MHz, DMSO-d_6) δ 11.8 (br s, 1H), 8.42 (br t, 1H), 7.8 (s, 1H), 7.43 (br s, 1H), 7.40−7.32 (m, 2H), 7.32−7.27 (m, 1H), 7.00 (br s, 1H), 6.91 (s, 1H), 6.90 (br t, 1H), 3.16−3.0 (m, 5H), 1.97−1.81 (m, 4H), 1.24 (t, J = 7.2 Hz, 3H); HRMS calcd for $C_{21}H_{24}ClN_5O$+H, 398.1742; found, 398.1742.

4-(4-(3-Chlorophenyl)-1*H*-pyrazol-3-yl)-*N*-phenyl-1*H*-pyrrole-2-carboxamide (5f). HPLC (Method A) t_R = 3.54 min; LC-MS (Method B) t_R = 3.2 min, 363.5 (M + 1), 361.5 (M − 1); LC-MS (Method C) t_R = 3.0 min, 363.1 (M + 1), 361.3 (M − 1); ^{1}H NMR (300 MHz, DMSO-d_6) δ 12.0 (br s, 1H), 9.8 (s, 1H), 7.72 (d, 3H), 7.46 (s, 1H), 7.38−7.29 (m, 6H), 7.15 (br s, 1H), 7.04 (t, 1H); HRMS calcd for $C_{20}H_{15}ClN_4O$+H, 363.1007; found, 363.1005.

N-Benzyl-4-(4-(3-chlorophenyl)-1*H*-pyrazol-3-yl)-1*H*-pyrrole-2-carboxamide (5g). HPLC (Method F) t_R = 10.1 min; MS calcd, 377.8; found, 377.4; ^{1}H NMR (500 MHz, CDCl$_3$) δ 7.7 (s, 1H), 7.4 (s, 1H), 7.3 (m, 5H), 7.25 (m, 3H), 6.95 (s, 1H), 6.8 (s, 1H), 4.55 (s, 1H).

4-(4-(3-Chlorophenyl)-1*H*-pyrazol-3-yl)-*N*-((pyridin-3-yl)-meth-yl)-1*H*-pyrrole-2-carboxamide (5h). HPLC (Method A) t_R = 2.69 min; LC-MS (Method B) t_R = 2.1 min, 378.5 (M + 1), 376.5 (M − 1); LC-MS (Method C) t_R = 2.5 min, 378.2 (M + 1), 376.3 (M − 1); ^{1}H NMR (300 MHz, DMSO-d_6) δ 11.7 (br s, 1H), 8.75 (t, 1H), 8.70 (br s, 1H), 8.61 (d, 1H), 8.05 (br d, 1H), 7.79 (s, 1H), 7.66 (br t, 1H), 7.43 (s, 1H), 7.38 (d, 2H), 7.29−7.26 (m, 1H), 6.98 (br s, 1H), 6.93 (br t, 1H), 4.5 (d, 2H); HRMS calcd for $C_{20}H_{16}$-ClN_5O+H, 378.1116; found, 378.1116. Anal. Calcd for $C_{24}H_{18}$-$ClF_6N_5O_5$·1.5H_2O: C, 45.55; H, 3.34; N, 11.07. Found: C, 45.30; H, 3.02; N, 10.88.

4-(4-(3-Chlorophenyl)-1*H*-pyrazol-3-yl)-*N*-((pyridin-4-yl)-meth-yl)-1*H*-pyrrole-2-carboxamide (5i). HPLC (Method F) t_R = 7.5 min; LC-MS (Method G) t_R = 4.9 min, 378.4 (M + 1), 376.3 (M − 1); ^{1}H NMR (500 MHz, CDCl$_3$) δ 8.5 (d, 2H), 8.65 (s, 1H), 7.45 (s, 1H), 7.3 (m, 5H), 6.95 (s, 1H), 6.85 (s, 1H), 4.6 (s, 2H).

N-Benzyl-4-(4-(3-chlorophenyl)-1*H*-pyrazol-3-yl)-*N*-methyl-1*H*-pyrrole-2-carboxamide (5j). HPLC (Method A) t_R = 3.59 min; LC-MS (Method B) t_R = 3.26 min, 391.5 (M + 1), 389.3 (M − 1); HPLC (Method C) t_R = 3.0 min, 391.3 (M + 1), 389.4 (M − 1); HRMS calcd for $C_{22}H_{19}ClN_4O$+H, 391.1320; found, 391.1320.

N-(3,4-Difluorobenzyl)-4-(4-(3-chlorophenyl)-1*H*-pyrazol-3-yl)-1*H*-pyrrole-2-carboxamide (5k). HPLC (Method A) t_R = 3.56 min; LC-MS (Method B) t_R = 3.2 min, 413.5 (M + 1), 411.5 (M − 1); LC-MS (Method C) t_R = 3.0 min, 413.2 (M + 1), 411.3 (M − 1); HRMS calcd for $C_{21}H_{15}ClF_2N_4O$+H, 413.0975; found, 413.0975.

N-(4-Methoxybenzyl)-4-(4-(3-chlorophenyl)-1*H*-pyrazol-3-yl)-1*H*-pyrrole-2-carboxamide (5l). HPLC (Method A) t_R = 3.43 min; LC-MS (Method B) t_R = 3.1 min, 407.6 (M + 1), 405.5 (M − 1); LC-MS (Method C) t_R = 2.9 min, 407.2 (M + 1), 405.3 (M − 1); HRMS calcd for $C_{22}H_{19}ClN_4O_2$+H, 407.1269; found, 407.1268.

4-(4-(3-Chlorophenyl)-1*H*-pyrazol-3-yl)-1*H*-pyrrol-2-yl)(3,4-dihydroisoquinolin-2-(1*H*)-yl)methane (5m). HPLC (Method A) t_R = 3.68 min; LC-MS (Method B) t_R = 3.3 min, 403.6 (M + 1), 401.5 (M − 1); LC-MS (Method C) t_R = 3.1 min, 403.2 (M + 1), 401.3 (M − 1); ^{1}H NMR (300 MHz, DMSO-d_6) δ 11.75 (s, 1H), 7.77 (s, 1H), 7.47 (br s, 1H), 7.40 (br d, 2H), 7.34−7.31 (m, 1H), 7.19 (s, 4H), 7.03 (br m, 1H), 6.67 (br s, 1H), 4.78 (s, 2H), 3.86 (br t, 2H), 2.86 (t, J = 5.7 Hz, 2H); HRMS calcd for $C_{23}H_{19}$-ClN_4O+H, 403.1320; found, 403.1319.

4-(4-(3-Chlorophenyl)-1*H*-pyrazol-3-yl)-*N*-(2-(pyridin-3-yl)-ethyl)-1*H*-pyrrole-2-carboxamide (5n). HPLC (Method A) t_R = 2.7 min; LC-MS (Method B) t_R = 2.0 min, 392.6 (M + 1), 390.5 (M − 1); LC-MS (Method C) t_R = 2.5 min, 392.2 (M + 1), 390.3 (M − 1); ^{1}H NMR (300 MHz, DMSO-d_6) δ 11.65 (s, 1H), 8.72 (s, 1H), 8.69 (d, J = 4.8 Hz, 1H), 8.25 (d, J = 7.8 Hz, 1H), 8.16 (br t, 1H), 7.84−7.79 (m, 2H), 7.42 (d, 1H), 7.36−7.32 (m, 2H), 7.30−7.27 (m, 1H), 6.94 (br s, 1H), 6.81 (br t, 1H), 3.52 (q, J = 6.3 Hz, 2H), 2.97 (t, J = 6.6 Hz, 2H); HRMS calcd for $C_{21}H_{18}ClN_5O$+H, 392.1273; found, 392.1271.

N-(Benzyloxy)-4-(4-(3-chlorophenyl)-1*H*-pyrazol-3-yl)-1*H*-pyrrole-2-carboxamide (5o). HPLC (Method A) t_R = 3.41 min; LC-MS (Method B) t_R = 3.0 min, 393.6 (M + 1), 391.5 (M − 1); LC-MS (Method C) t_R = 2.9 min, 393.2 (M + 1), 391.3 (M − 1); HRMS calcd for $C_{21}H_{17}ClN_4O_2$+H, 393.1113; found, 393.1112.

4-(4-(3-Chlorophenyl)-1*H*-pyrazol-3-yl)-*N*-((R)-1-phenylethyl)-1*H*-pyrrole-2-carboxamide (6a). HPLC (Method A) t_R = 3.57 min; LC-MS (Method B) t_R = 3.2 min, 391.6 (M + 1), 389.5 (M − 1); LC-MS (Method C) t_R = 3.0 min, 391.2 (M + 1), 389.4 (M − 1). ^{1}H NMR (300 MHz, DMSO-d_6) δ 11.6 (s, 1H), 8.4 (d, J = 8.1 Hz, 1H), 7.8 (s, 1H), 7.45 (br s, 1H), 7.37−7.18 (m, 9H), 7.05 (s, 1H), 6.94 (br m, 1H), 5.13 (p, J = 7.5 Hz, 1H), 1.44 (d,

$J = 6.9$ Hz, 3H); HRMS calcd for $C_{22}H_{19}ClN_4O+H$, 391.1320; found, 391.1319. Anal. Calcd for $C_{24}H_{20}ClF_3N_4O_3 \cdot 1.5H_2O$: C, 54.19; H, 4.36; N, 10.53. Found: C, 54.36; H, 4.56; N, 10.31.

4-(4-(3-Chlorophenyl)-1*H*-pyrazol-3-yl)-*N*-((S)-1-phenylethyl)-1*H*-pyrrole-2-carboxamide (6b). HPLC (Method A) $t_R = 3.57$ min; LC-MS (Method B) $t_R = 3.2$ min, 391.6 (M + 1), 389.5 (M − 1); LC-MS (Method C) $t_R = 3.0$ min, 391.2 (M + 1), 389.4 (M − 1); ^{1}H NMR (300 MHz, DMSO-d_6) δ 11.6 (s, 1H), 8.43 (d, $J = 8.1$ Hz, 1H), 7.80 (s, 1H), 7.45 (s, 1H), 7.37−7.28 (m, 8H), 7.23−7.19 (m, 1H), 7.05 (s, 1H), 6.94 (br m, 1H), 5.13 (p, $J = 7.8$ Hz, 1H), 1.44 (d, $J = 6.9$ Hz, 3H); HRMS calcd for $C_{22}H_{19}$-ClN_4O+H, 391.1320; found, 391.1319.

4-(4-(3-Chlorophenyl)-1*H*-pyrazol-3-yl)-*N*-((S)-2-hydroxy-1-phenylethyl)-1*H*-pyrrole-2-carboxamide (6c). HPLC (Method A) $t_R = 3.23$ min; LC-MS (Method B) $t_R = 2.9$ min, 407.6 (M + 1), 405.5 (M − 1); LC-MS (Method C) $t_R = 2.7$ min, 407.1 (M + 1), 405.3 (M − 1); HRMS calcd for $C_{22}H_{19}ClN_4O_2+H$, 407.1269; found, 407.1270.

(S)-2-(4-(4-(3-Chlorophenyl)-1*H*-pyrazol-3-yl)-1*H*-pyrrole-2-carboxamido)-2-phenylacetic acid (6d). HPLC (Method D) $t_R = 6.2$ min; MS 421.0 (M + 1), 419.0 (M − 1).

N-((S)-Carbamoyl(phenyl)methyl)-4-(4-(3-chlorophenyl)-1*H*-pyrazol-3-yl)-1*H*-pyrrole-2-carboxamide (6e). HPLC (Method A) $t_R = 3.15$ min; LC-MS (Method B) $t_R = 2.8$ min, 420.6 (M + 1), 418.5 (M − 1); LC-MS (Method C) $t_R = 2.6$ min, 420.1 (M + 1), 418.3 (M − 1); HRMS calcd for $C_{22}H_{18}ClN_5O_2+H$, 420.1222; found, 420.1220.

N-((S)-(Methylcarbamoyl(phenyl)methyl)-4-(4-(3-chlorophenyl)-1*H*-pyrazol-3-yl)-1*H*-pyrrole-2-carboxamide (6f). HPLC (Method D) $t_R = 6.0$ min; LC-MS (Method E) $t_R = 3.0$ min, 434.0 (M + 1), 432.0 (M − 1).

4-(4-(3-Chlorophenyl)-1*H*-pyrazol-3-yl)-*N*-(2,3-dihydro-2-hydroxy-1*H*-inden-1-yl)-1*H*-pyrrole-2-carboxamide (6g). HPLC (Method A) $t_R = 3.3$ min; LC-MS (Method B) $t_R = 2.9$ min, 419.4 (M + 1), 417.3 (M − 1); LC-MS (Method C) $t_R = 2.7$ min, 419.2 (M + 1), 417.3 (M − 1); ^{1}H NMR (300 MHz, DMSO-d_6) δ 11.65 (s, 1H), 8.39 (d, $J = 8.4$ Hz, 1H), 7.79 (s, 1H), 7.44 (s, 1H), 7.36−7.34 (m, 2H), 7.27−7.25 (m, 1H), 7.09 (br d, 1H), 6.98 (br s, 2H), 5.25 (t, $J = 7.8$ Hz, 1H), 4.33 (q, $J = 7.2$ Hz, 1H), 3.20−3.11 (m, 1H), 2.76−2.71 (m, 1H); HRMS calcd for $C_{23}H_{19}ClN_4O_2+H$, 419.1269; found, 419.1270.

4-(4-(3-Chlorophenyl)-1*H*-pyrazol-3-yl)-*N*-(1-(4-fluorophenyl)-2-hydroxyethyl)-1*H*-pyrrole-2-carboxamide (6h). HPLC (Method A) $t_R = 3.31$ min; LC-MS (Method B) $t_R = 2.9$ min, 425.6 (M + 1), 423.5 (M − 1); LC-MS (Method C) $t_R = 2.7$ min, 425.1 (M + 1), 423.3 (M − 1); ^{1}H NMR (300 MHz, DMSO-d_6) δ 11.65 (s, 1H), 8.31 (d, $J = 8.4$ Hz, 1H), 7.80 (s, 1H), 7.45 (br s, 1H), 7.42−7.35 (m, 4H), 7.31−7.26 (m, 1H), 7.13 (t, 2H), 7.05 (br s, 1H), 6.94 (br m, 1H), 5.06 (q, $J = 6.9$ Hz, 1H), 3.70 (CH$_2$ obscured by H$_2$O); HRMS calcd for $C_{22}H_{18}ClFN_4O_2+H$, 425.1175; found, 425.1172. Anal. Calcd for $C_{24}H_{19}ClF_4N_4O_4 \cdot 0.5H_2O$: C, 52.61; H, 3.68; N, 10.23. Found: C, 52.46; H, 3.37; N, 10.18.

4-(4-(3-Chlorophenyl)-1*H*-pyrazol-3-yl)-*N*-(1-(4-chlorophenyl)-2-hydroxyethyl)-1*H*-pyrrole-2-carboxamide (6i). HPLC (Method A) $t_R = 3.43$ min; LC-MS (Method B) $t_R = 3.1$ min, 441.5 (M + 1), 439.5 (M − 1); LC-MS (Method C) $t_R = 2.8$ min, 441.1 (M + 1), 439.3 (M − 1); HRMS calcd for $C_{22}H_{18}Cl_2N_4O_2+H$, 441.0879; found, 441.0880.

4-(4-(3-Chlorophenyl)-1*H*-pyrazol-3-yl)-*N*-(1-(4-(trifluoro-methyl)phenyl)-2-hydroxy-ethyl)-1*H*-pyrrole-2-carboxamide (6j). HPLC (Method A) $t_R = 3.54$ min; LC-MS (Method B) $t_R = 3.1$ min, 475.6 (M + 1), 473.5 (M − 1); LC-MS (Method C) $t_R = 2.9$ min, 475.2 (M + 1), 475.3 (M − 1); HRMS calcd for $C_{23}H_{18}$-$ClF_3N_4O_2+H$, 475.1143; found, 475.1145.

4-(4-(3-Chlorophenyl)-1*H*-pyrazol-3-yl)-*N*-(1-(2-fluorophenyl)-2-hydroxyethyl)-1*H*-pyrrole-2-carboxamide (6k). HPLC (Method A) $t_R = 3.28$ min; LC-MS (Method B) $t_R = 2.9$ min, 425.6 (M + 1), 423.5 (M − 1); LC-MS (Method C) $t_R = 2.7$ min, 425.1 (M + 1), 423.3 (M − 1). ^{1}H NMR (500 MHz, acetone-d_6) δ 7.85 (m, 2H), 7.5 (s, 1H), 7.4 (m, 2H), 7.35 (t, 1H), 7.25 (m, 3H), 7.1 (m, 2H), 5.2 (t, 1H), 3.8 (m, 2H); ^{1}H NMR (300 MHz, DMSO-d_6) δ 11.70 (s, 1H), 8.36 (d, $J = 8.1$ Hz, 1H), 7.80 (s, 1H), 7.45−7.42 (m, 2H), 7.37−7.35 (br d, 2H), 7.30−7.26 (m, 2H), 7.18−7.11 (m, 2H), 7.08 (s, 1H), 6.94 (br s, 1H), 5.34 (q, $J = 7.5$ Hz, 1H), 3.80 (CH$_2$ obscured by H$_2$O); HRMS calcd for $C_{22}H_{18}ClFN_4O_2+H$, 425.1175; found, 425.1171. Anal. Calcd for $C_{26}H_{20}ClF_7N_4O_6 \cdot 0.5H_2O$: C, 47.18; H, 3.20; N, 8.46. Found: C, 47.28; H, 3.23; N, 9.04.

4-(4-(3-Chlorophenyl)-1*H*-pyrazol-3-yl)-*N*-(1-(3-fluorophenyl)-2-hydroxyethyl)-1*H*-pyrrole-2-carboxamide (6l). HPLC (Method D) $t_R = 5.6$ min; LC-MS (Method E) $t_R = 2.9$ min, 425.1 (M + 1), 423.1 (M − 1).

4-(4-(3-Chlorophenyl)-1*H*-pyrazol-3-yl)-*N*-(1-(3,4-difluorophenyl)-2-hydroxyethyl)-1*H*-pyrrole-2-carboxamide (6m). HPLC (Method A) $t_R = 3.36$ min; LC-MS (Method B) $t_R = 3.0$ min, 443.6 (M + 1), 441.5 (M − 1). LC-MS (Method C) $t_R = 2.7$ min, 443.2 (M + 1), 441.3 (M − 1). ^{1}H NMR (500 MHz, acetone-d_6) δ 7.9 (s, 1H), 7.65 (s, 1H), 7.5 (br d, 1H), 7.4 (br d, 2H), 7.35 (br d, 1H), 7.3 (t, 2H), 7.25 (t, 1H), 7.15 (br s, 1H), 7.1 (br s, 1H), 5.2 (br t, 1H), 3.8 (d, 2H); HRMS calcd for $C_{22}H_{18}ClF_2N_4O_2+H$, 443.1081; found, 443.1083.

4-(4-(3-Chlorophenyl)-1*H*-pyrazol-3-yl)-*N*-(1-(3,5-dichlorophenyl)-2-hydroxyethyl)-1*H*-pyrrole-2-carboxamide (6n). HPLC (Method D) $t_R = 7.1$ min; LC-MS (Method E) $t_R = 3.5$ min, 476.8 (M + 1), 474.8 (M − 1).

N-(1-(3-Chloro-4-fluorophenyl)-2-hydroxyethyl)-4-(4-(3-chlorophenyl)-1*H*-pyrazol-3-yl)-1*H*-pyrrole-2-carboxamide (6o). HPLC (Method D) $t_R = 6.5$ min; LC-MS (Method E) $t_R = 3.3$ min, 458.9 (M + 1), 457.0 (M − 1).

Compounds **6p** and **6q** were isolated after chromatography using a chiral column: ChiralPack AD column, 4.5×250 mm; eluting with a 40% mixture of isopropanol and hexanes over 18 min run time; flow rate 1 mL/min; 254 nM. Compound **6p** eluted first at 8.4 min, followed by **6q** at 12.6 min.

N-((S)-1-(3-Chloro-4-fluorophenyl)-2-hydroxyethyl)-4-(4-(3-chlorophenyl)-1*H*-pyrazol-3-yl)-1*H*-pyrrole-2-carboxamide (6p). HPLC (Method A) $t_R = 3.47$ min; LC-MS (Method B) $t_R = 3.1$ min, 459.5 (M + 1), 457.5 (M − 1); LC-MS (Method C) $t_R = 2.8$ min, 459.1 (M + 1), 457.3 (M − 1); ^{1}H NMR (300 MHz, DMSO-d_6) δ 11.70 (s, 1H), 8.35 (d, $J = 8.1$ Hz, 1H), 7.80 (s, 1H), 7.56 (d, $J = 7.5$ Hz, 1H), 7.45 (s, 1H), 7.37−7.35 (m, 4H), 7.30−7.26 (m, 2H), 7.06 (s, 1H), 6.94 (br s, 1H), 5.04 (q, $J = 7.8$ Hz, 1H), 3.80 (CH$_2$ obscured by H$_2$O); HRMS for calcd for $C_{22}H_{17}Cl_2FN_4O_2+H$, 459.0785; found, 459.0783. Anal. Calcd for $C_{24}H_{18}Cl_2F_4N_4O_4 \cdot H_2O$: C, 48.75; H, 3.41; N, 9.47. Found: C, 48.58; H, 3.41; N, 9.26.

N-((R)-1-(3-Chloro-4-fluorophenyl)-2-hydroxyethyl)-4-(4-(3-chlorophenyl)-1*H*-pyrazol-3-yl)-1*H*-pyrrole-2-carboxamide (6q). HPLC (Method A) $t_R = 3.47$ min; LC-MS (Method B) $t_R = 3.1$ min, 459.5 (M + 1), 457.5 (M − 1); LC-MS (Method C) $t_R = 2.8$ min, 459.1 (M + 1), 457.3 (M − 1).

Supporting Information Available: Experimental details on compound characterization; biochemical and biological procedures; crystallization conditions; and data collection statistics. This material is available free of charge via the Internet at http://pubs.acs.org.

References

(1) Jemal, A.; Murray, T.; Ward, E.; Samuels, A.; Tiwari, R. C.; Ghafoor, A.; Feuer, E. J.; Thun, M. J. Cancer statistics, 2005. *Ca−Cancer J. Clin.* **2005**, *55*, 10−30.

(2) Thambi, P.; Sausville, E. A. STI571 (imatinib mesylate): The tale of a targeted therapy. *Anticancer Drugs* **2002**, *13*, 111−114.

(3) Putz, T.; Culig, Z.; Eder, I. E.; Nessler-Menardi, C.; Bartsch, G.; Grunicke, H.; Uberall, F.; Klocker, H. Epidermal growth factor (EGF) receptor blockade inhibits the action of EGF, insulin-like growth factor I, and a protein kinase A activator on the mitogen-activated protein kinase pathway in prostate cancer cell lines. *Cancer Res.* **1999**, *59*, 227−233.

(4) Hynes, N. E.; Lane, H. A. ERBB receptors and cancer: The complexity of targeted inhibitors. *Nat. Rev. Cancer* **2005**, *5*, 341−354.

(5) Tse, K. F.; Mukherjee, G.; Small, D. Constitutive activation of FLT3 stimulates multiple intracellular signal transducers and results in transformation. *Leukemia* **2000**, *14*, 1766−1776.

(6) Bos, J. L. *ras* Oncogenes in human cancer: A review. *Cancer Res.* **1989**, *49*, 4682−4689.

(7) Mercer, K. E.; Pritchard, C. A. Raf proteins and cancer: B-Raf is identified as a mutational target. *Biochim. Biophys. Acta* **2003**, *1653*, 25−40.

(8) Sebolt-Leopold, J. S.; Herrera, R. Targeting the mitogen-activated protein kinase cascade to treat cancer. *Nat. Rev. Cancer* **2004**, *4*, 937−947.

(9) Smalley, K. S. A pivotal role for ERK in the oncogenic behaviour of malignant melanoma? *Int. J. Cancer* **2003**, *104*, 527−532.

(10) Kohno, M.; Pouyssegur, J. Pharmacological inhibitors of the ERK signaling pathway: Application as anticancer drugs. *Prog. Cell Cycle Res.* **2003**, *5*, 219−224.

(11) Chang, F.; Steelman, L. S.; Shelton, J. G.; Lee, J. T.; Navolanic, P. M.; Blalock, W. L.; Franklin, R.; McCubrey, J. A. Regulation of cell cycle progression and apoptosis by the Ras/Raf/MEK/ERK pathway (Review). *Int. J. Oncol.* **2003**, *22*, 469−480.

(12) Hilger, R. A.; Scheulen, M. E.; Strumberg, D. The Ras-Raf-MEK-ERK pathway in the treatment of cancer. *Onkologie* **2002**, *25*, 511−518.

(13) Investigational Drugs Database; Thomson Scientific, Ltd., 2006.

(14) (*S*)-*N*-(2,3-Dihydroxypropoxy)-3,4-difluoro-2-(2-fluoro-4-iodophenylamino)benzamide: Kaufman, M. D.; Barrett, S. D.; Flamme, C. M.; Warmus, J.; Smith, Y. D.; Cheriyan, M.; Zhang, L.; Tecle, H.; Sebolt-Leopold, J. S.; Valik, H.; Gowan, R.; Van Becelaere, K.; Merriman, R.; Przybranowski, S.; Ohren, J.; Whitehead, C.; Leopold, W. R.; Dobrusin, E.; Bridges, A. Synthesis and SAR development of PD 0325901, a potent and highly bioavailable MEK inhibitor. *Proc. Am. Assoc. Cancer Res.* **2004**, *45*, Abst. 2477.

(15) 5-(4-Bromo-2-chlorophenylamino)-4-fluoro-*N*-(2-hydroxyethoxy)-1-methyl-1*H*-benzo[d]imidazole-6-carboxamide: Wallace, E.; Yeh, T.; Lyssikatos, J.; Winkler, J.; Lee, P.; Marlow, A.; Hurley, B.; Marsh, V.; Bernat, B.; Evans, R.; Colwell, H.; Parry, J.; Baker, S.; Ballard, J.; Morales, T.; Smith, D.; Brandhuber, B.; Gross, S.; Poch, G.; Litwiler, K.; Hingorani, G.; Otten, J.; Sullivan, F.; Blake, J.; Rizzi, J.; Pheneger, T.; Goyette, M.; Koch, K. Preclinical development of ARRY-142886, a potent and selective MEK inhibitor. *Proc. Am. Assoc. Cancer Res.* **2004**, *45*, Abst. 3891.

(16) Green, J.; Cao, J.; Hale, M.; Baker, C.; Maltais, F.; Janetka, J.; Mullican, M.; Bemis, G.; Xie, X.; Straub, J.; Tang, Q.; Mashall, R. Pyrazole compositions useful as inhibitors of ERK. WO 01/57022, 2001.

(17) Tang, Q.; Maltais, F.; Janetka, J.; Hale, M. Pyrazole-derived kinase inhibitors and uses thereof. WO 03/011854, 2003.

(18) Hale, M.; Janetka, J.; Maltais, F.; Tang, Q. Pyrazole-derived kinase inhibitors and uses thereof. WO 03/011855, 2003.

(19) Vieth, M.; Higgs, R. E.; Robertson, D. H.; Shapiro, M.; Gragg, E. A.; Hemmerle, H. Kinomics-structural biology and chemogenomics of kinase inhibitors and targets. *Biochim. Biophys. Acta* **2004**, *1697*, 243−257.

(20) Nagar, B.; Bornmann, W. G.; Pellicena, P.; Schindler, T.; Veach, D. R.; Miller, W. T.; Clarkson, B.; Kuriyan, J. Crystal structures of the kinase domain of c-Abl in complex with the small molecule inhibitors PD173955 and imatinib (STI-571). *Cancer Res.* **2002**, *62*, 4236−4243.

(21) Atwell, S.; Adams, J. M.; Badger, J.; Buchanan, M. D.; Feil, I. K.; Froning, K. J.; Gao, X.; Hendle, J.; Keegan, K.; Leon, B. C.; Muller-Dieckmann, H. J.; Nienaber, V. L.; Noland, B. W.; Post, K.; Rajashankar, K. R.; Ramos, A.; Russell, M.; Burley, S. K.; Buchanan, S. G. A novel mode of Gleevec binding is revealed by the structure of spleen tyrosine kinase. *J. Biol. Chem.* **2004**, *279*, 55827−55832.

(22) Mol, C. D.; Dougan, D. R.; Schneider, T. R.; Skene, R. J.; Kraus, M. L.; Scheibe, D. N.; Snell, G. P.; Zou, H.; Sang, B. C.; Wilson, K. P. Structural basis for the autoinhibition and STI-571 inhibition of c-Kit tyrosine kinase. *J. Biol. Chem.* **2004**, *279*, 31655−31663.

(23) Cowan-Jacob, S. W.; Fendrich, G.; Manley, P. W.; Jahnke, W.; Fabbro, D.; Liebetanz, J.; Meyer, T. The crystal structure of a c-Src complex in an active conformation suggests possible steps in c-Src activation. *Structure* **2005**, *13*, 861−871.

(24) Heathcock, C. H.; Norman, M. H.; Dickman, D. A. Total synthesis of (.+-.)-vallesamidine. *J. Org. Chem.* **1990**, *55*, 798−811.

(25) Feenstrar, R. W.; Stokkingreef, E. H. M.; Reichwein, A. M.; Lousberg, W. B. H.; Ottenheijm, H. C. J.; Kamphuis, J.; Boesten, W. H. J.; Schoemaker, H. E.; Meijer, E. M. Oxidative preparation of optically active *n*-hydroxy-α-amino acid amides. *Tetrahedron* **1990**, *46* (5), 1745−1756.

(26) Donner, B. G. Conversion of chiral amino acids to enantiomerically pure α-methylamines. *Tetrahedron Lett.* **1995**, *36*, 1223−1226.

JM061381F